AT&T Technical Journal
Vol. 64, No. 10, December 1985
Printed in U.S.A.

A Laboratory Simulation Facility for Multipath Fading Microwave Radio Channels

By A. J. RUSTAKO, JR., C. B. WOODWORTH, R. S. ROMAN, and H. H. HOFFMAN*

(Manuscript received April 29, 1985)

This paper describes a laboratory facility capable of simulating time-varying radio multipath channel responses in real time under computer control. Four independent fading channels are available that can be used for single-polarization nondiversity, combined in pairs for single-polarization dual diversity, or cross-coupled to simulate the two outputs of a dual-polarization nondiversity channel. Each channel contains a controllable variable network capable of producing a narrowband intermediate frequency response that resembles the "three-path" function of Rummler. A wide range of models can be accommodated by altering the computer-stored sequences used to control each variable channel network. The only assumption implicit in the choice of model is that the channel response can be fitted to the generic function over bandwidths up to 40 MHz. The channel responses are controlled by either entering fixed parameters from a keyboard, or by reading time-varying parameters stored in disk memory. This description includes the architecture, hardware design, software implementation, and performance of the simulation facility.

I. INTRODUCTION

1.1 Motivation

The primary impediment to the operation of digital radio on microwave line-of-sight paths is multipath fading. In dual-polarization

* Authors are employees of AT&T Bell Laboratories.

(dual-pol) systems, this problem is augmented by cross-polarization (cross-pol) coupling. Numerous radio measurements and data analyses over the past several years have served to characterize multipath and cross-pol responses, and to translate these characterizations into statistical models.[1-11] Many of these models have been eagerly engaged by radio systems analysts to estimate, using analysis and/or Monte Carlo simulation, the expected link outage times for different modulations, link parameters and receiver techniques.[12-22] Over the same period, a number of outage measurements have been reported for specific hardware designs, based on either field trials conducted over radio paths or laboratory "signature" measurements coupled with assumed radio channel models.[23-31]

If one stands back from this myriad of activities, important limitations in all of the above approaches become apparent. The analysis/simulation of statistical models applied to specified designs permits rapid comparisons among contending radio schemes, but relies on idealized models of the hardware behavior. Moreover, such study methods do not readily take account of the time dynamics of the channel responses. The coupling of statistical models with lab-measured hardware "signatures" likewise omits channel time dynamics and their effects on system techniques. This deficiency is absent only in the case of field measurements, but these are both costly and time-consuming. More important, system qualities inferred from this approach are subject to the particular responses that nature provides during the test interval. Meaningful comparisons between systems, therefore, require measurements conducted in parallel under identical conditions of path and time.

The Channel Simulation Facility (CSF) reported here is intended to fill the gaps between these various study approaches. It simulates time-varying radio channel responses in the laboratory in real time, and it plays the channel responses into actual hardware realizations rather than idealized system models. The channel responses are dictated by computer-generated control signals, and so the twin benefits of *model selectability* (software-controllable changes in the history of the channel response functions) and *repeatability* (ability to replicate the channel response history for different systems at different times) are realized. And, finally, the ability to simulate channels in a laboratory can sharply contract the time needed to cover a "fading year" and permit considerable reductions in cost.

1.2 Features of the CSF

The heart of the CSF is a group of four identical, variable channel networks, each of which produces, under computer control, a narrow-

band Intermediate Frequency (IF) response that resembles the "three-path" function of Rummler.[1] That function is commonly expressed in the literature as

$$H(f) = a[1 - be^{j\phi}e^{-j\omega\tau}]; \qquad \tau = 6.3 \text{ ns}, \tag{1}$$

where a, b and ϕ are slowly varying random "fade parameters," and $\omega(= 2\pi f)$ is measured from the selected intermediate frequency. For later convenience, the following parameters are defined:

$$A = -20 \log_{10} a \tag{2}$$

$$B = -20 \log_{10}(1 - b). \tag{3}$$

Thus each variable network has a response about the IF (either 70 MHz or 1.070 GHz, as selected) given by

$$H(f) = a + ce^{j\theta}e^{-j\omega\tau}, \tag{4}$$

where a and c are computer-controlled attenuations and θ is a computer-controlled phase shift. In terms of (1), the hardware variables c and θ are ab and $\phi + \pi$, respectively. For later convenience, we define

$$C = -20 \log_{10} c. \tag{5}$$

The four variable channel networks are physically paired, i.e., two such networks with a common input but separate outputs are contained in each of two identical Dual Channel Units (DCUs). The four networks can be used in three distinct ways: (1) A single network (any of the four) can be used to produce the output of a single-pol nondiversity channel, e.g., see Fig. 1a; (2) two networks within the same DCU can be used to produce the two outputs of a single-pol dual diversity channel, e.g., see Fig. 1b; or (3) all four networks can be combined, using a Cross-Coupling Unit (CCU), to produce the two outputs of a dual-pol nondiversity channel, e.g., see Fig. 2.

We thus see that a total of three units comprise the CSF, permitting either of three modes of use at either of two IFs. These and other features of the CSF are summarized in Table I.

Two important facts about the CSF are important to emphasize. One is that the responses of the four networks are completely and separately controllable, and can be driven either via specified hardware parameters typed into a computer terminal (dial-up responses, which are fixed until the input parameters are changed); or via software control, whereby the electronically adjustable hardware parameters are time varied by reading stored sequences from a disk and applying Digital-To-Analog (D/A) conversion and low-pass filtering. In the latter case, the sequences are produced by software routines tailored to a specified statistical channel model. A wide range of models can

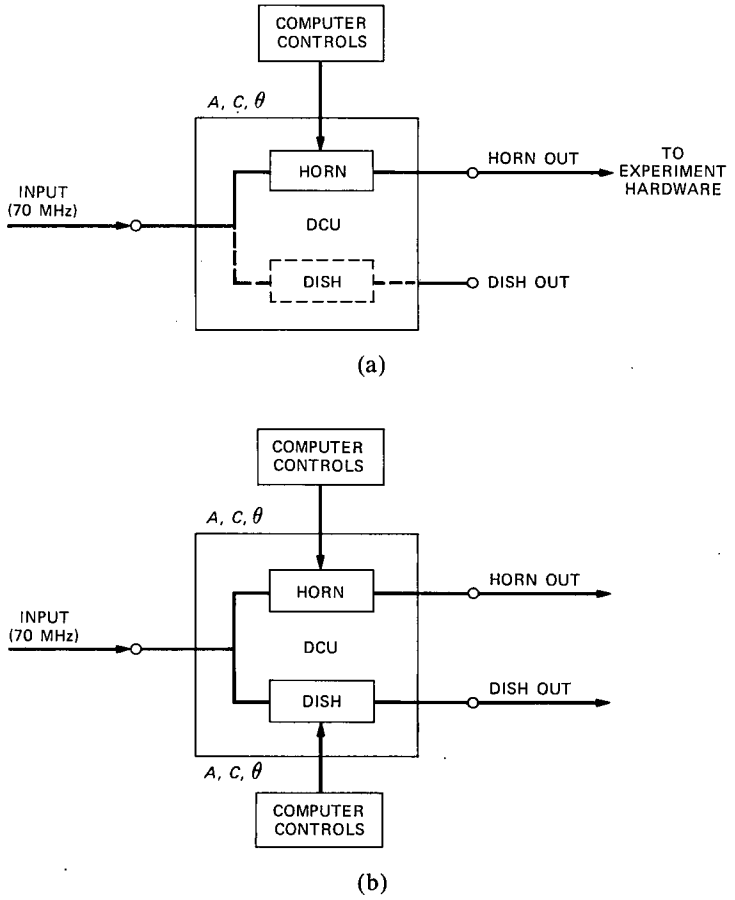

Fig. 1—Simulation modes of (a) a single-pol channel nondiversity and (b) a dual space diversity.

thus be accommodated by suitably altering the software routines. This feature is the key to the flexibility and simplicity of use of the CSF.

The second important fact is that designing the variable networks about the "three-path" function is *not* restrictive with respect to permissible channel models. The *only* assumption implicit in this approach is that all channel response functions of interest can be well fitted by this generic function. For the vast majority of radio paths that have been measured, the evidence supports this assumption for channel bandwidths up to 40 MHz. This means that if a given user of the CSF wishes to consider a model with a different fitting function (e.g., the first-degree polynomial[3] or the "two-path" function[10]), software can be written to interface this model with the simulator hardware.

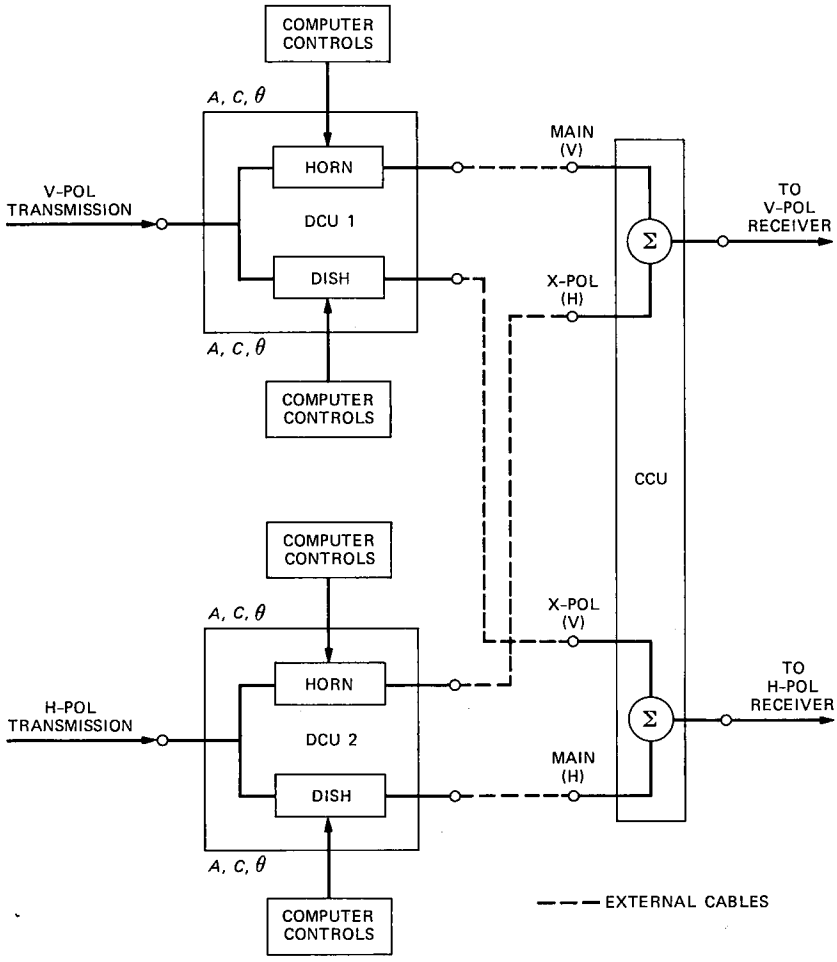

Fig. 2—Simulation mode of a dual-pol nondiversity channel.

1.3 Outline of the remaining material

Section II describes the architecture of the CSF, showing block diagrams of the three main units and discussing how they are used to provide the various possible modes of operation. Section III gives a more detailed description of the electronic circuits and components, while Section IV gives details on the construction. Section V discusses the software associated with the CSF. Specific topics include the generation of the sequences that drive the variable hardware parameters, and the calibration and measurement of the variable networks. The existing software for generating the sequences is tailored to a specific dual-diversity channel model. Section VI presents perform-

Table I—Definitions and some features of the channel simulation facility

Capabilities	Simulates either a single-pol nondiversity channel (1 input, 1 output); a single-pol diversity channel (1 input, 2 outputs); or a dual-pol nondiversity channel (2 inputs, 2 outputs).
Physical configuration	Consists of two identical dual channel units (DCUs) and one cross-connecting unit (CCU), plus connecting cables.
DCU (Multipath fade simulator)	Contains two parallel networks (common input, separate outputs), each producing a separate, variable "three-path" frequency response.
CCU ("Cross-pol coupler")	Connects the four outputs of two DCUs so as to simulate a dual-pol nondiversity channel.
Variability of the network responses	Computer-controlled; either keyboard entry fixed responses or program-generated time-varying responses.
Input IF	70 MHz
Input power level	0 dBm
Output IF	70 MHz or 1.070 GHz, as selected.
Output power	0 dBm for each variable channel network at 70 MHz. −15 dBm for each variable channel network at 1.070 GHz.
Bandwidth	Each network provides a "three-path" response over ±20 MHz about the intermediate frequency.

ance results. This includes specific data on bandwidths, power levels and calibration stability; assessments of how well the computer-generated sequences satisfy the underlying statistical model; and assessments of how well the hardware response variations match the intended ones, i.e., those dictated by the computer-generated outputs.

II. ARCHITECTURE

2.1 Dual channel units

Figure 3 shows, in simplified form, the block diagram of a DCU. A DCU contains two parallel networks with a common IF input, the top network being labeled *Horn Channel* and the bottom are being labeled *Dish Channel.* These labels are particularly apt when the two networks simulate the two paths of a dual space diversity link. For convenience, we will use these designations throughout our discussions to distinguish the top and bottom networks.

An actual DCU contains circuitry not depicted in Fig. 3, including bandlimiting IF filtering, upconversions from 70 MHz to 1.070 GHz, and the provision of the variable phase shifts (θ) via local oscillators and mixers. This circuitry will be discussed in Section III.

A control computer is used to control, through D/A conversion and low-pass filtering, each of the circuit parameter a, c and θ. It is thus

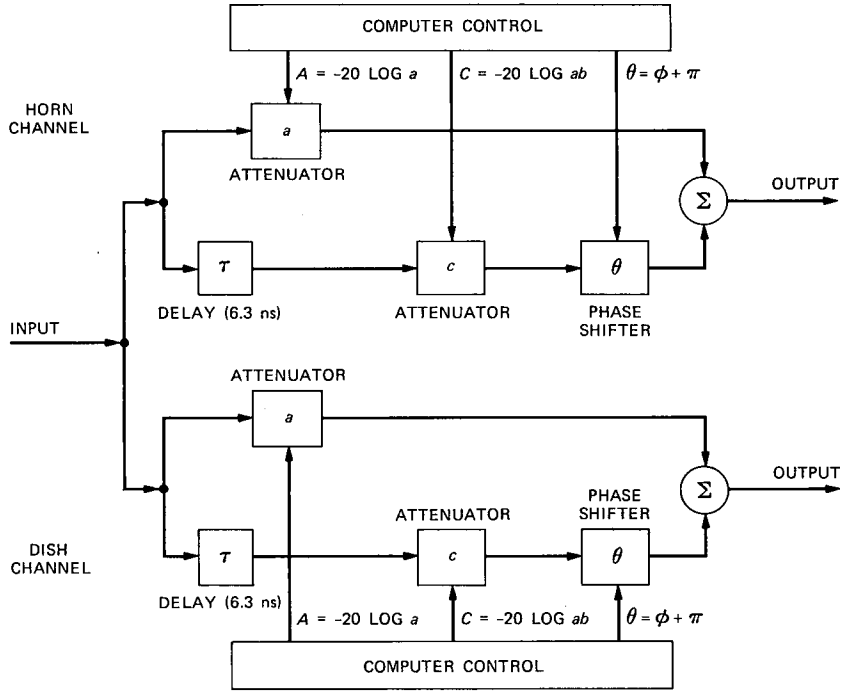

Fig. 3—Simplified block diagram of a dual channel unit.

clear that each of the two networks provides a frequency response identical in form to (4).

Finally, Fig. 3 shows the manner in which the intermediate frequency of the network outputs is selected. When the external connecting cables (shown dashed) are absent, the two outputs are at 1.070 GHz. When the cables are connected as shown, each 1.070-GHz output is applied to a separate downconverter, with a shared 1.0-GHz Local Oscillator (LO) providing the other input. In this case, the outputs will be at 70 MHz, the IF of the DCU input.

2.2 Modes of operation

Figure 1 shows two obvious ways to use a single DCU. In Fig. 1a, the control computer delivers fade parameters (A, C and θ) to just the Horn Channel network, and the output of just that network is applied to the follow-on equipment. Alternatively, one could control, and use the output from, just the Dish Channel. In either case, the simulator is used in this way to represent a single-pol nondiversity channel.

In Fig. 1b, the control computer delivers fade parameters to both the Horn *and* Dish Channel networks, and both outputs are used. In this case, the simulator can be configured as a dual space diversity

channel. On a typical space diversity link, the primary (upper) and secondary (lower) receiving antennas on the radio tower would be of the horn and dish type, respectively, thus leading to the designations used here.

Finally, Fig. 2 shows how two DCUs, combined with a CCU (described shortly) can be used to represent a dual-pol nondiversity channel: The path from the V-pol transmitter to the V-pol receiver passes through the Horn Channel of DCU 1. The interfering path from that transmitter into the H-pol receiver passes through the Dish Channel of the same DCU 1. Similarly, the H-pol path to the H-pol and V-pol receivers passes through the Dish and Horn Channels, respectively, of DCU 2.

It should be mentioned that the two IF inputs in Fig. 2 need not be frequency synchronous. In most practical dual-pol systems, the dually polarized signals have the same *nominal* carrier, but the carriers are not identical unless the same Radio Frequency (RF) source is used for each. The arrangement of Fig. 2 is amenable to either possibility. To complete the picture, we now describe the internal pathways of the CCU.

2.3 The cross-coupling unit

Figure 4 shows how the CCU combines four inputs to produce the simulated V-pol and H-pol outputs of a dual-pol channel: the co-pol V and cross-pol H signals are combined in a 10-dB directional coupler, following a manually set attenuation and phase shift of the latter, to produce the V-pol receiver input. Similar combining produces the H-pol receiver input.

The manual attenuation adjustments in the CCU, achieved via panel-mounted controls, extend the dynamic range over which the cross-pol coupling levels can be varied. Each attenuator can be incremented in 1-dB steps from 0 dB to 43 dB.

The manual phase shift adjustments, also achieved via panel-mounted controls, provide flexibility in how the co-pol and cross-pol signals from the same original transmission are relatively phased. The phase adjustment is continuous over a range of nearly 360 degrees.

III. CIRCUIT DESIGN

3.1 General

The CSF could have been designed in any number of ways. We have taken a particular approach that combines practical circuitry, wide bandwidth, accurate performance and operational flexibility. We will elaborate here on some of the circuitry that comprises a DCU. The circuitry of the CCU was adequately described in the previous section.

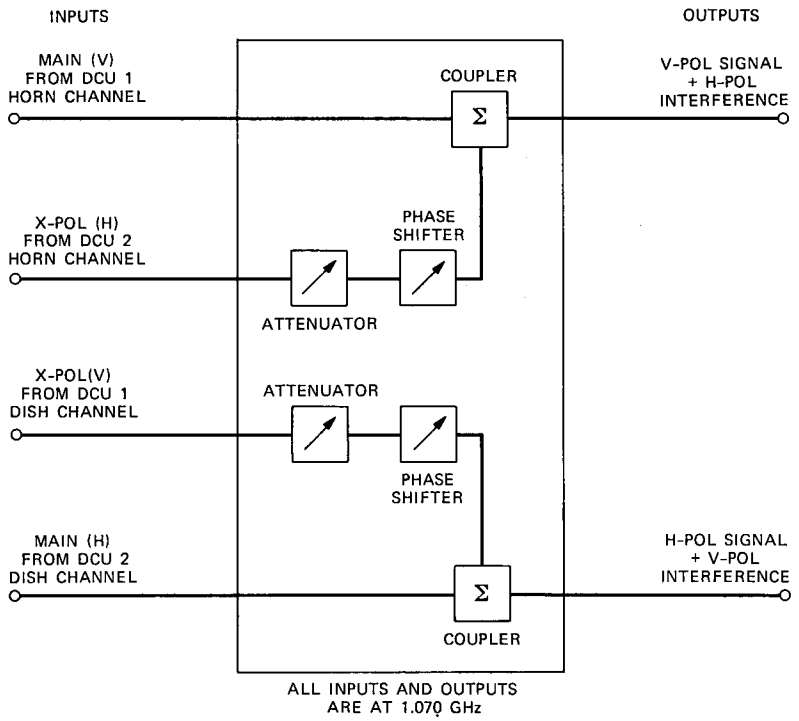

Fig. 4—Block diagram of the cross-coupling unit.

Each variable channel network of a DCU contains a direct path with a variable (analog voltage controlled) attenuator, and a parallel path with a 6.3-ns delay, a variable attenuator *and* a variable (analog voltage controlled) phase shifter. The summed outputs of these paths yield a network response akin to the "three path" function of Rummler. Each of the parallel paths must be nondispersive, in fact, over a bandwidth of 40 MHz or more. Further, it should be possible to vary each attenuator without introducing phase changes and to vary the phase shifter without introducing attenuation changes.

An input frequency of 70 MHz and a channel bandwidth of 40 MHz were chosen for the CSF. The variable channel networks could be built at this or any other frequency if ideal components were available. However, given the limitations of practical components, we chose the approach of converting the input signal frequency to a higher frequency, where narrowband circuit techniques can be used. This approach, moreover, simplifies the task of providing the variable phase shift, as we shall see.

A network frequency of 1.070 GHz was chosen. This choice trades off the availability of "phase shift free" narrowband attenuators, and

ease of filtering of unwanted mixing products and local oscillator leakage through the mixer. The network output at 1.070 GHz can be either downconverted back to 70 MHz, used directly, or easily upconverted to, say, 4, 6, or 11 GHz for radio equipment tests.

3.2 The variable channel network

A simplified block diagram of a single variable channel network is shown in Fig. 5. The input signal at 70 MHz (Point 1) is power divided into two paths. One component is upconverted in a double-balanced diode mixer to 1.070 GHz; the other is delayed and then similarly upconverted to 1.070 GHz by a second double-balanced diode mixer. The output from the first mixer is controlled in amplitude by a variable attenuator and provides one input to a signal combiner. The output from the second mixer (in the delayed path) is controlled in amplitude by a second attenuator and in relative phase by the local oscillator phase shifter. This delayed signal sums with the direct input in the output signal combiner.

The 6.3-ns delay is provided by adding additional coaxial cable in the 70-MHz signal path between the input power divider and the delayed path upconverter. The exact length of this cable is determined empirically by measuring the signal delay difference at the output signal combiner (points 2 and 3). This is most easily done in the frequency domain by sweeping the network input signal, setting the

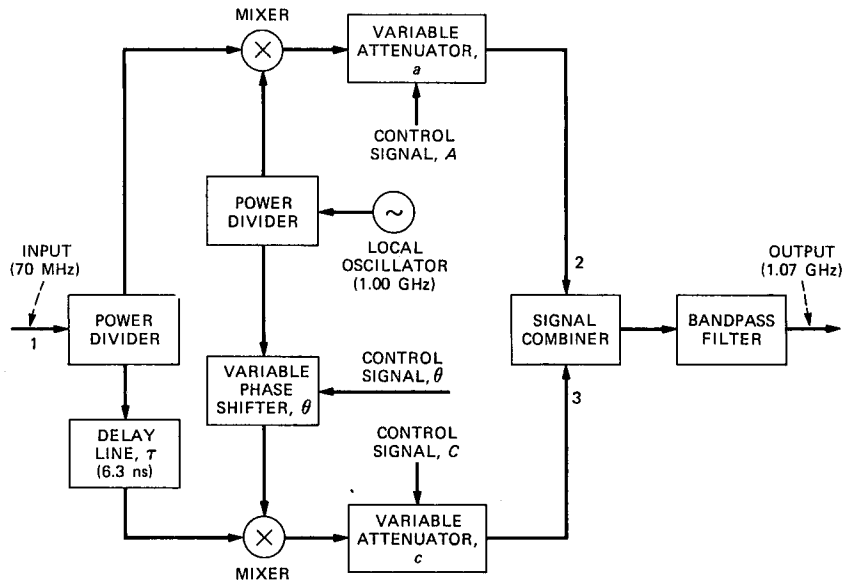

Fig. 5—Simplified block diagram of a single variable channel network.

direct path and delayed path attenuations to be about equal (to form periodic deep fades), and then measuring the frequency spacing between successive nulls. When the path difference is 6.3 ns, the null spacing is 158.73 MHz, which is the reciprocal of the delay.

The output of the variable channel network contains both the upper and lower mixing products at 1.070 GHz and 0.930 GHz. If the 1.070-GHz signal is to be mixed back to 70 MHz, the contribution from the 0.930-GHz signal will distort the desired channel response and must be effectively eliminated by filtering.

3.3 Detailed description of a DCU

A detailed block diagram of a DCU is shown in Fig. 6. This diagram shows the two variable channel networks driven by a common 70-MHz input signal and the two downconverters for mixing the simulator outputs back to the input frequency. A crystal-controlled phase-locked Continuous Wave (CW) source at 1 GHz acts as a common local oscillator to all upconverters and downconverters, to ensure frequency coherence between the input signal and both output signals. When both DCUs are used in the complete CSF, they are virtually identical except for the provision to drive all four variable channel networks from a common local oscillator residing in one DCU (master). This higher power source in the master DCU can drive the second DCU (slave). The result is four frequency-coherent outputs, assuming the input signals to the two DCUs are themselves frequency coherent. (As described in Section 2.2, the two input signals to the DCUs may or may not be frequency coherent, depending on the experiment.)

Each variable network uses two local oscillator signals for upconversion. One is derived through power dividers from the 1-GHz source; the other passes first through a voltage-controlled phase shifter. The phase shifter varies the phase of the 1-GHz CW signal from 0 degrees to over 360 degrees, when the θ control signal varies between 0 and +10 volts. This phase is imparted to the signal in the delayed path of the variable network by the mixing process of the upconverter.

The signals are scaled in the direct and delayed paths of each variable channel network by voltage-controlled attenuators. The attenuations are variable from 0 dB to over 36 dB when the A and C control signals vary between 0 and +10 volts. The outputs from the attenuators are added in a reactive signal combiner. The combined signal is bandpass filtered to eliminate the lower mixing product at 0.930 GHz. The desired output from the filter at 1.070 GHz is amplified to provide the final fading channel output.

The output filter, a fifth-order Butterworth filter with a 3-dB bandwidth of 70 MHz, is the most narrowband circuit of each variable network. This filter adequately attenuates the unwanted mixing prod-

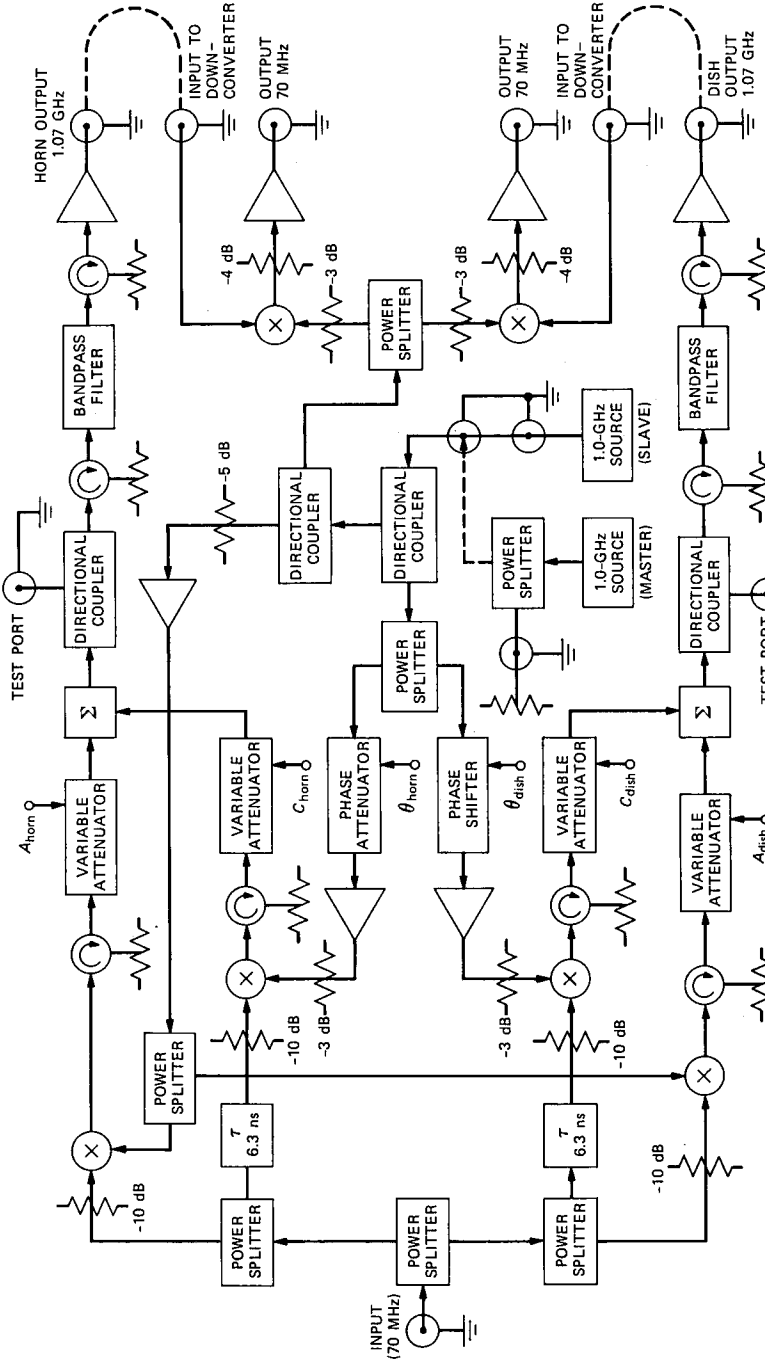

Fig. 6—Detailed block diagram of a dual channel unit.

uct while maintaining a flat amplitude response with small time delay variation (±1.5 ns) over the design bandwidth of 40 MHz.

Care was taken to isolate components in the various signal paths, to prevent reflections from mismatches that produce unwanted ripples in the channel response. Fixed coaxial attenuators and ferrite isolators were used where necessary to minimize reflections.

3.4 Interface circuits

As we have seen, the four attenuators and two phase shifters within each DCU are controlled by time-varying analog voltages, the latter being derived from digital sequences supplied by the control computer. To accomplish this, two D/A converters mounted within the computer provide six control voltage sequences to each DCU. Each sequence consists of 12-bit words delivered at a 1-Hz rate. Each sequence is converted into a smooth analog variation by a fourth-order Butterworth state variable low-pass filter with a 3-dB bandwidth of 0.5 Hz.

IV. CONSTRUCTION

4.1 Construction of the DCU

Figure 7 shows a top view of the inside of a DCU. Semirigid coaxial

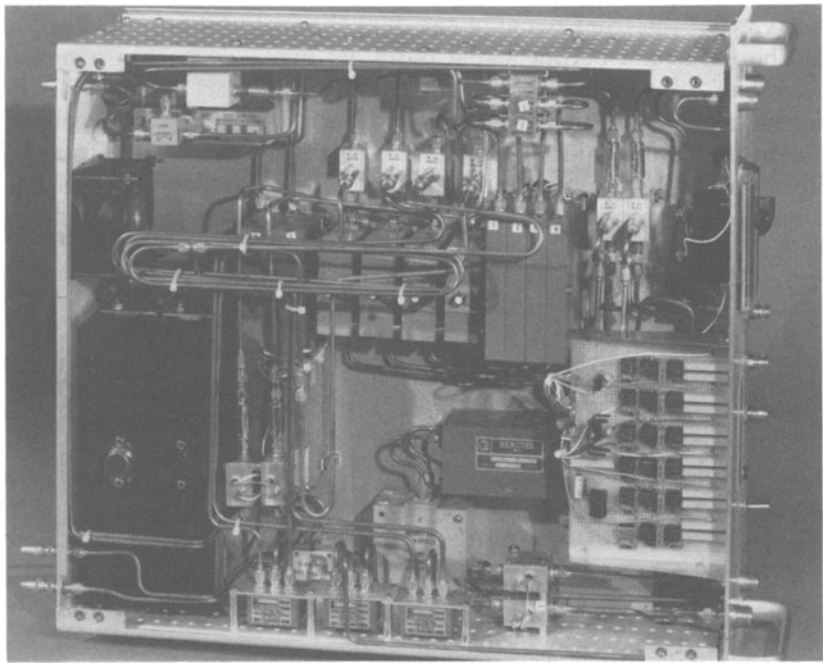

Fig. 7—Top view of the inside of a dual channel unit.

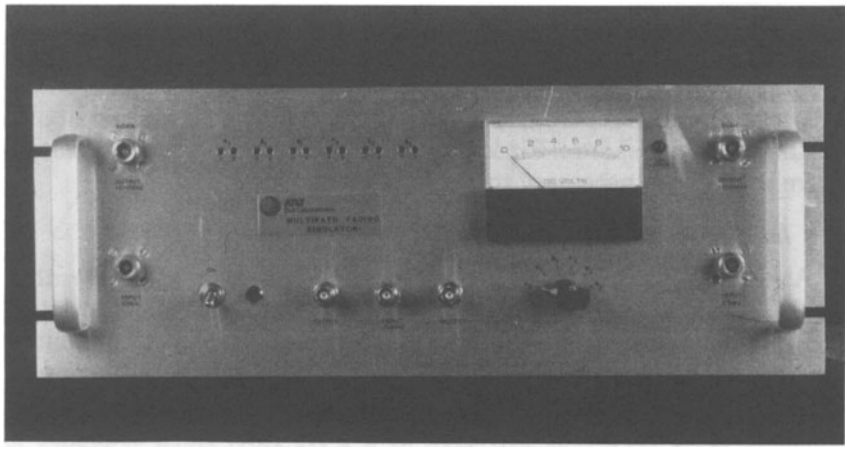

Fig. 8—Front view of a dual channel unit.

line (.141 inch) was used to interconnect components to improve phase stability. Line lengths in both the direct and delay paths were closely matched in each variable channel network of each DCU, so as to obtain nearly identical characteristics. The elongated coils in the center of the figure are the additional line lengths required to produce the 6.3-ns path delays.

A view of the front panel of the dual channel unit is shown in Fig. 8. The input and output signal ports are available on the panel for interconnection convenience. The 70-MHz input port and the 70-MHz downconverter output ports are the three BNC-type coaxial connectors in the lower center of the panel. The 1.070-GHz outputs from the Horn and Dish variable channel networks are brought out on N-type coaxial connectors located at the upper left and upper right sides of the panel. The inputs to the two downconverters associated with the Horn and Dish channels are located directly below these N-type connectors.

Screw-trimmer adjustments, paired in 12 holes in the upper center left of the panel, are provided for shifting and scaling the control voltages to the four variable attenuators and two phase shifters. The range of these control voltages is approximately preset by adjustments on the D/A converter boards within the control computer. The front panel adjustments allow for convenient trimming at the DCU. The panel meter can be selectively switched to monitor each of these voltages.

4.2 Construction of the CCU

Figures 9 and 10 show a top view of the inside and the front panel of the cross-coupling unit. This relatively simple unit contains the two

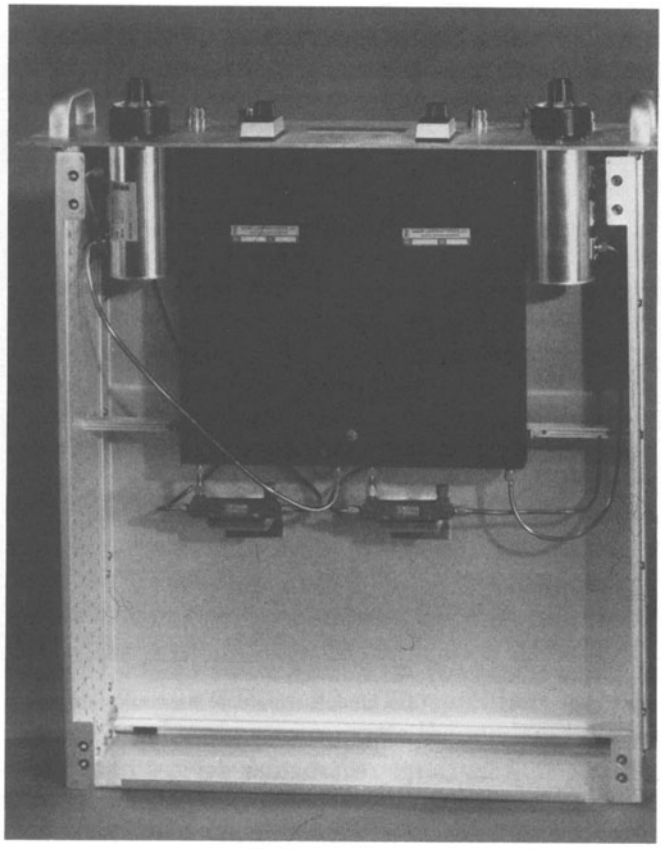

Fig. 9—Top view of the inside of the cross-coupling unit.

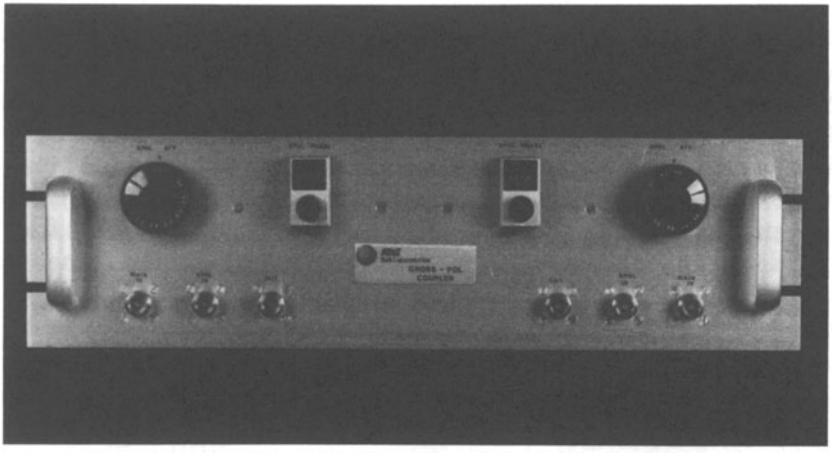

Fig. 10—Front view of the cross-coupling unit.

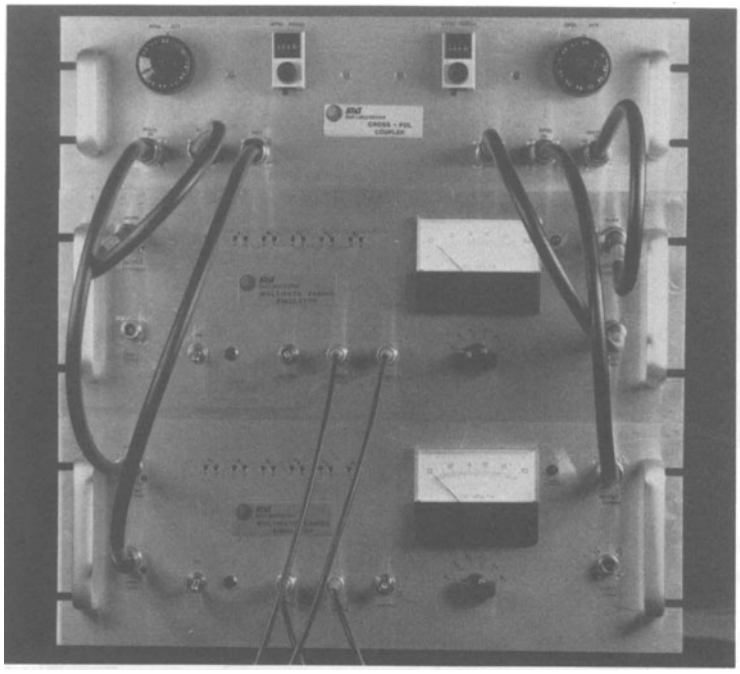

Fig. 11—Front view of the complete channel simulation facility.

cross-pol phase shifters (large rectangular devices in the center), the two cross-pol attenuators (cylindrical devices adjacent to the phase shifters) and two 10-dB directional couplers.

4.3 Interconnections for the CSF

The front view of the complete CSF is shown in Fig. 11. The cable interconnections shown represent the cross-coupled case described in Section 2.2. The lower DCU can be arbitrarily called the V-pol channel and the upper DCU, the H-pol channel. The V-pol Horn Channel output is connected to the left cross-pol coupler Main input. The H-pol Horn Channel output is connected to the left cross-pol coupler X-Pol input, to be attenuated and phase-shifted before summing to the main V-pol signal. The dish and horn outputs from the H-pol and V-pol channels, respectively, are similarly combined in the right cross-pol coupler. The cross-pol coupler outputs are shown returned to the respective downconverters in the DCUs to provide 70-MHz outputs. If desired, instead, the 1.070-GHz outputs from the coupler can be used directly.

V. SOFTWARE DESIGN

This section deals with two distinct aspects of the CSF software.

One is the computer routines that generate random time sequences for parameters of the specified channel models; the other is the software that runs on the control computer to effect real-time operation of the CSF hardware.

The sequence generation software was developed on the *UNIX*™ operating system with the option to move it to the control computer. In the initial arrangement, however, the fade parameter sequences were generated on a *UNIX* system minicomputer and down loaded to the control computer. As described earlier, these sequences were converted into continuous analog signals and played into the simulator hardware to achieve time-varying channel responses. Special software was written to test the accuracy of the generated sequences and of the resulting hardware responses. These issues are dealt with in Section VI.

5.1 Generating the random fade parameter sequences

We describe here how to generate the random time-varying parameters for a fade model. We will first summarize the generation procedure employed by our software to generate random variations with any given Probability Density Function (PDF) and Autocorrelation Function (ACF). Then we will describe the techniques used to generate random variations with PDFs and ACFs specified by Rummler.[7] In this subsection, we show how to generate the random variations A, B, and ϕ, as defined in (2), for both the Horn and Dish Channels. The transformation of these variations into A, C, and θ is performed by the control computer and is described briefly in a later section on control computer software.

5.1.1 Iterative random variation generation method

The problem of generating a random variation with arbitrary PDF and ACF is difficult in general and sometimes impossible.[32] In our case, however, we wish to match the statistics of fade models with well-behaved PDFs and ACFs. Further, while accurate matching of the PDF is essential, particularly when the simulator is used for outage measurements, slight variations in the ACF shape are acceptable since the ACF is either unknown or only sparsely measured for many models. These considerations ease the variation generation problem considerably. It should be noted that the second-order statistics are not uniquely determined by the PDF and ACF and that we will accept whatever second-order statistics are generated when matching the PDF and ACF.

This method is general in that it generates random variations with any specified PDF and with an ACF close to the specified ACF. The method starts by generating a Gaussian random process with an initial

ACF that we normally take as the desired ACF. From the Gaussian variation, a new variation with the required PDF can be formed by a nonlinear transformation. It is easier to think of this transformation in two steps—a Gaussian-to-uniform transformation followed by a transformation to the required PDF. The first transformation involves using the Q function, while the second transformation involves using the inverse of the required distribution function. While this gives variations with the correct PDF, the nonlinear transformations will make the output ACF different from the initial ACF.

To make the output ACF match the desired ACF, we use the following iterative procedure: The initial ACF is applied to the underlying Gaussian variation. Based on the output ACF and an educated guess, we select a new ACF for the underlying Gaussian variation. This procedure stops when the desired ACF is obtained. In our case, the iterative procedure converges quickly. We found that the ACFs of two of our parameters remained essentially unchanged after the nonlinear transformations.

We describe the first part of this procedure in detail here and in the following subsection, and continue the detailed discussion by way of an example for clarity. We begin the procedure by generating a Gaussian variation. Many techniques can be used here and are well known, although we chose one similar to that used by Vannucci and Teich.[33] The ACF for the Gaussian variation generation is initialized, usually to the desired ACF.

The nonlinear transformation required to convert the Gaussian variations into variations with the desired PDF is broken up into a transformation to uniform followed by a transformation to the desired PDF. The transformation to uniform can be accomplished through the Q function, i.e.,

$$u = Q(x) = \frac{1}{\sqrt{2}} \int_{-\infty}^{x} e^{-\frac{y^2}{2}} dy, \tag{6}$$

where x is the original Gaussian variation and u is the uniform variation. This function can also be used as a test of the quality of the Gaussian variation by computing the new probability distribution function and comparing the result with the uniform probability distribution function. This test was used to verify the uniform-to-Gaussian random variation conversions.

5.1.2 Implementation of a space diversity fade model

We chose to use the Rummler dual-channel space diversity fade model,[7] although Rummler's rationalized model[8] or any other dual channel model could have been employed as well. Familiarity with Rummler models is assumed in the following paragraphs.

Since ACF measurements are not available for this model but are available for the single-channel model,[34] we use the single-channel model ACFs for both channels of the diversity model. These ACFs, measured by Rummler, are not true ACFs; they were rescaled so that $R(0) = 1$. The scaling factor was determined by extrapolating the measured ACF to the ordinate and finding the intercept. The ACF for each of the fade parameters closely approximates an exponential. For this reason, we applied an exponential ACF to each underlying Gaussian variation and adjusted its time constant to form different ACFs. Matching the time constants at the $1/e$ points of the rescaled Rummler ACFs gives time constants of 129, 53, and 32 seconds for the respective A, B, and ϕ parameters. These ACFs were used in generating the underlying Gaussian variation discussed above.

The easiest parameters to generate are the ϕ's because they are independent of each other and of all the other parameters. For each ϕ, we begin with $U(0, 1)$ variation, u, generated as discussed in the previous subsection. The ϕ parameter, with a pedestal-type PDF, is generated from the u variation by the simple rescaling

$$\phi(u) = \begin{cases} 90(1 + \alpha)(2u - 1)/\alpha; & |2u - 1)| \leq \alpha/(1 + \alpha) \\ 90(1 + \alpha)(2u - 1) + 90(1 - \alpha)\text{sgn}(2u - 1); & \text{otherwise,} \end{cases} \quad (7)$$

where α is the pedestal parameter (5 for the Horn Channel and 8 for the Dish Channel) and ϕ is in degrees.

The B parameters are generated next because, in both the Horn and Dish Channels, the A parameter's mean value is dependent on the B parameter. The general technique for converting a $U(0, 1)$ random variation to a particular distribution can be accomplished by passing each sample through the inverse of the distribution function. For the B parameters, finding the inverse function algebraically is rather complicated, so this was done numerically.

Finally, the A parameters are generated. For this case, the final distribution is Gaussian so no transformations are need to obtain the correct PDF. However, the mean of each A is dependent on the associated value of B. Further, A_{horn} is correlated with A_{dish}. To generate the A's, two independent $N(0, 1)$ random variations (x_1 and x_2) with identical ACFs are generated. Next, they are linearly combined to produce the desired correlation and, finally, the variances are scaled and appropriate mean values are added. In short,

$$A_{\text{horn}} = \sigma_{\text{horn}} x_1 + \mu_{\text{horn}}(B_{\text{horn}}) \quad (8)$$

$$A_{\text{dish}} = \rho\sigma_{\text{dish}} x_1 + \sigma_{\text{dish}} \sqrt{1 - \rho^2} x_2 + \mu_{\text{dish}}(B_{\text{dish}}), \quad (9)$$

where the Greek constants and the $\mu(B)$ functions are defined in Ref. 7.

5.2 Control computer software

The control computer software falls into two categories, namely software to produce the fades and software to calibrate and test the hardware. The purpose of the fade software is (1) to translate fade model variations (e.g., A, B, and ϕ) into the A, C, and θ variations supported by the hardware; (2) to perform calibration table lookup and quantization to the closest binary output sample value; and (3) to play the binary variations through the analog hardware. The remaining software generates the calibration tables, tests the overall accuracy of the fade control and calibration software, as well as the analog hardware, and allows manual control over the fade simulator. These operations are described in more detail in the following subsections.

5.2.1 Control computer—fade software

The analog hardware implements the transfer function given by (4), (see Fig. 5), where $c = ab$ and $\theta = \phi + \pi$. The voltage-controlled attenuators have control signals proportional to 10 log (power attenuation). These final log conversions are handled by a lookup table (described shortly), but the software-generated parameters A and B are in decibel form and must first be converted to linear form before computing c. The phase offset of π is required in the hardware to ensure continuity into the D/A low-pass filter.

To ensure accuracy, calibration lookup tables are used to map and quantize the analog floating point values generated from the fade model software into one of the integer output values of the D/A converter. Software automatically finds the closest table entry to the floating point value and outputs the corresponding integer value. Separate software outputs these integer variations from RAM memory or disk to the D/A converters at a 1-Hz rate.

5.2.2 Control computer—calibration and test software

The calibration lookup tables discussed above are automatically generated under software control via hardware measurements taken with a network analyzer connected to a computer. The a and c parameter calibrations are similar as shown in Figs. 12a and b and require the disconnection and termination of the delayed path (direct path for the c parameter). The control computer then measures the end-to-end attenuation of the connected path for each of the 4096 values and generates a table. These values are smoothed by averaging within a window centered around each value. This is required to obtain a monotonic table, especially for large attenuations where measurements become noisy.

To simplify the software, the θ calibration was made interactive. With both paths connected as in Fig. 12c, a spectral dip or notch is

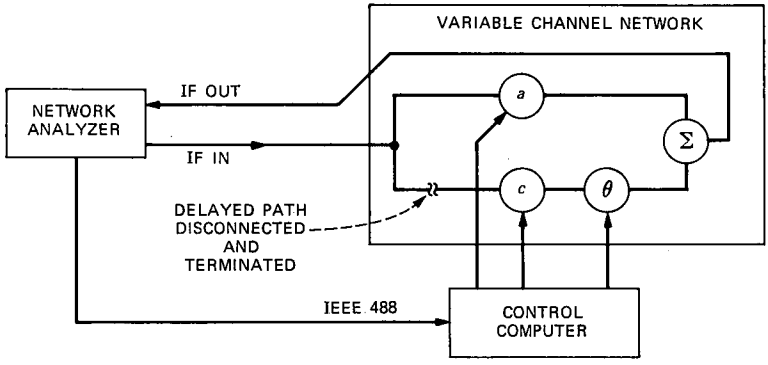

(a) CALIBRATION OF *a*

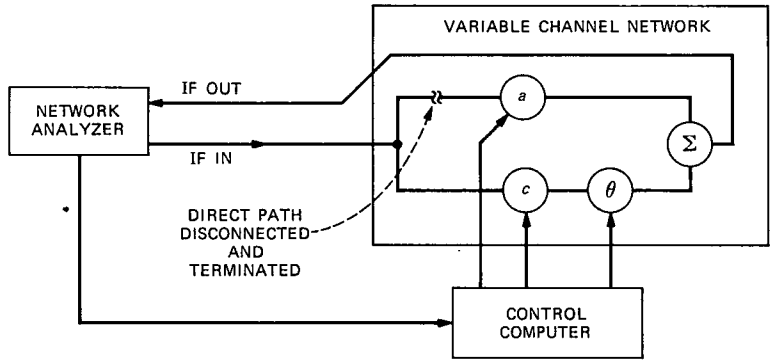

(b) CALIBRATION OF *c*

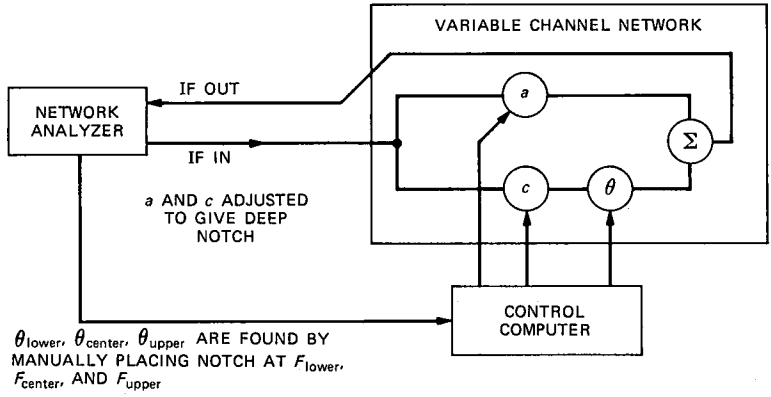

(c) CALIBRATION OF θ

Fig. 12—Block diagrams of parameter calibrations: (a) calibration of a, (b) calibration of c, and (c) calibration of θ.

formed by manually adjusting the relative values of a and c. This notch is placed at the upper and lower band edges as well as the center of the channel and the binary control values are stored. This information is then used to generate the lookup table via interpolation and extrapolation. The extrapolation is needed since notch position measurements can only be made in the bandlimited channel.

Additional software allows for manual control over each of the parameters, A, C, and θ, in real time. This provides for quick checking of the hardware and the lookup tables. This software also provides a useful mode of operation for the simulator, allowing selected responses to be easily "dialed" into the hardware.

Finally, there is software for playing a selected response and comparing it with the actual response measured by the network analyzer to obtain an error measure. More details about this are contained in the performance section that follows.

VI. PERFORMANCE

We will evaluate the performance of the CSF in several ways here. First, we illustrate some "three-path" responses produced by the variable channel networks over the 40-MHz bandwidth of interest. Next, we demonstrate that the joint statistics of the computer-generated sequences of fade variables (A, B and ϕ) conform to the model from which they are derived. Finally, we demonstrate that the frequency responses of the hardware, over a computer-generated population of A, C, θ values, are indeed the responses these fade variables are intended to produce. With these demonstrations, we affirm that the CSF can produce laboratory fading environments similar to those on actual digital radio links.

6.1 Channel frequency responses

The static and dynamic transmission performance of each DCU was measured using a Hewlett-Packard Model 8505A Network Analyzer. Here we discuss frequency response measurements on one or both variable channel networks of a DCU, and show sample results.

In a typical measurement, fixed control voltages are set by keyboard inputs on the control computer, and applied to the attenuators and phase shifters of the variable channel networks. The values of the control voltages produce a particular transmission function in each network. The Network Analyzer provides a frequency-swept input signal, in the vicinity of 70 MHz, to the DCU. The two 70-MHz outputs from the DCU are returned to the analyzer, where the frequency response magnitudes of the two networks are simultaneously observed. Alternatively, only one network output from the DCU is returned to the analyzer, along with a reference sample of the input

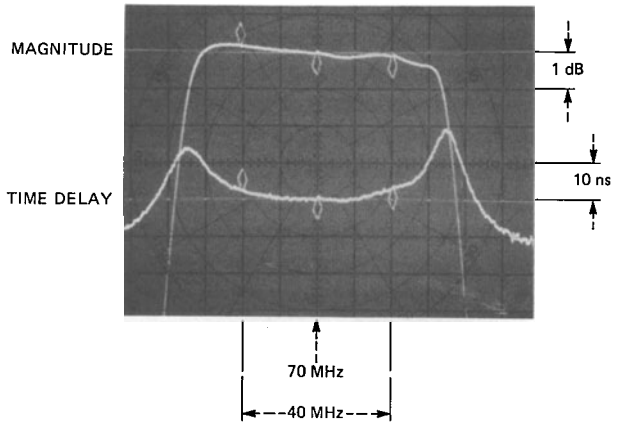

Fig. 13—Frequency response of one channel of a dual channel unit.

signal, to permit measurement of both the transmission magnitude *and* phase (or group delay) of that network.

In our initial experiment, we set the control voltage of the delay path attenuator so as to give maximum attenuation (>36 dB). This enabled us to measure the transmission performance of the direct path alone, with the output filter and downconverter included. Figure 13 shows the corresponding frequency response for one channel of a DCU. The upper trace is the magnitude and the lower trace is the group delay. Over a 40-MHz bandwidth centered at 70 MHz, the magnitude is flat within ±0.12 dB and the group delay is flat within ±1.5 ns. This response is primarily determined by the output Butterworth filter described in Section 3.3.

In another experiment, we set the control voltage to the delay path attenuator so that the signal level at the variable channel network combiner was 0.92 dB weaker than that of the direct path. A minimum-phase fade was thus created, with a maximum fade depth 20 dB below the direct path gain. The upper trace in Fig. 14 shows the magnitude of the resulting response. The delay path phase shifter was set to place the maximum fade in the center of the channel passband. The lower trace shows the channel group delay, wherein the time delay distortion can be clearly seen: Frequency components at the edges of the channel are delayed by more than 60 ns relative to components in the center of the channel.

When the signal levels in the direct and delay paths are interchanged so that the delayed signal to the network combiner is 0.92 dB *stronger*,

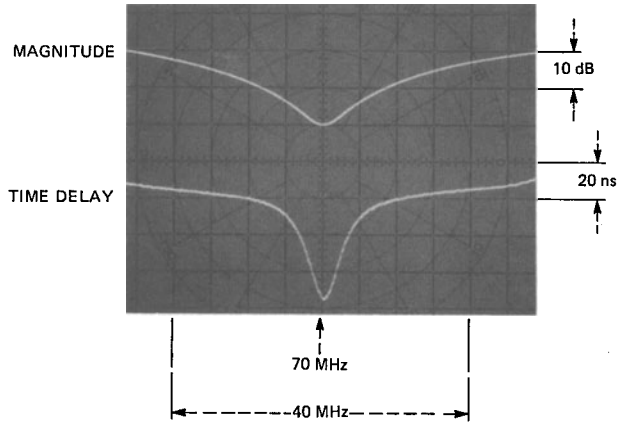

Fig. 14—A single-channel response for a 20-dB minimum phase fade.

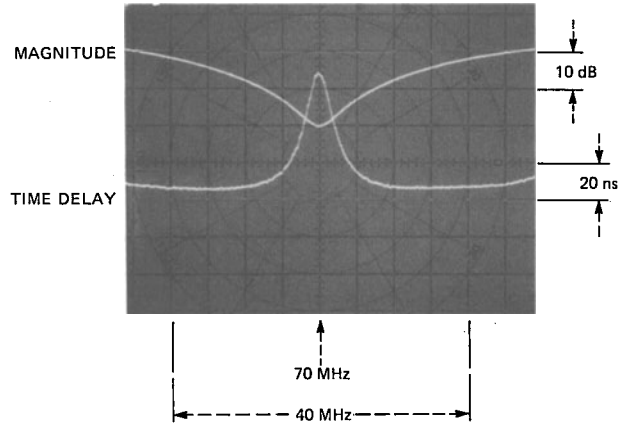

Fig. 15—A single-channel response for a 20-dB nonminimum phase fade.

a nonminimum-phase fade occurs, with the same maximum fade depth of 20 dB. The upper trace in Fig. 15 shows the transmission magnitude of the resulting channel response, with the maximum fade placed once more in the center of the channel passband. The time delay distortion is shown in the lower trace. Under these conditions, signal components at the center of the channel are delayed relative to components at the edges of the channel.

In general, by appropriately setting the relative signal levels in the direct and delay paths of a variable channel network, the depth of fade in the channel response can be selected. This fade can then be positioned in frequency by appropriately setting the phase shift in the delay path. Figure 16a shows the transmission magnitude of the

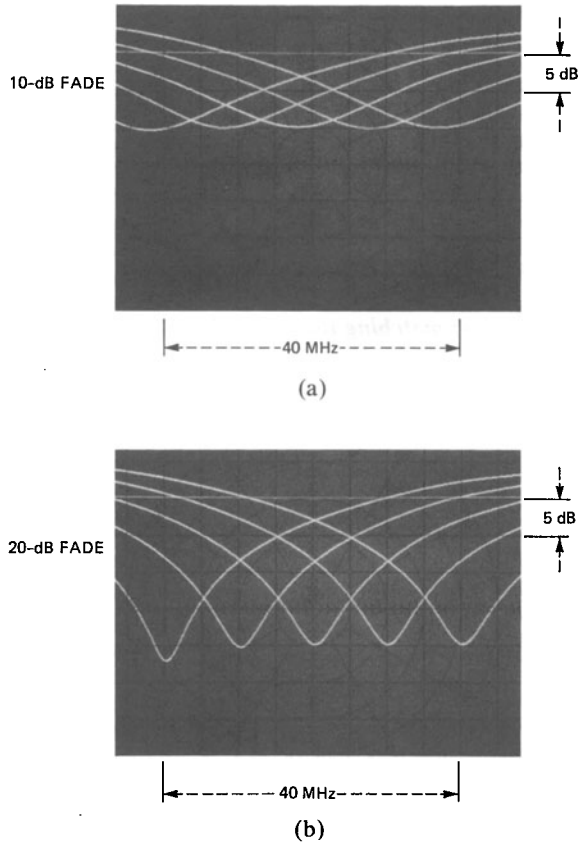

Fig. 16—Transmission magnitude response as a fade is moved in frequency across channel.

channel response as a 10-dB fade is moved in frequency across the channel. The fade depth remains constant within better than ±0.25 dB over the 40-MHz channel bandwidth. If the delay path signal level is increased in magnitude to produce a 20-dB fade depth, the variation in fade depth across the channel increases to ±1.0 dB, as shown in Fig. 16b. These variations are due to minor amplitude response imbalances between the direct and delay paths. The ±1.0-dB variation for a 20-dB fade depth, for example, is caused by imbalances of about ±0.1 dB.

6.2 Signal levels

The DCU was designed to be a general-purpose laboratory instrument. A nominal input signal level of 0 dBm was chosen for the 70-MHz DCU input. This level is normally available from the modulator

portion of typical radio modems. The unfaded 70-MHz output from each network of the DCU is designed to have a level of 0 dBm when there is 3-dB attenuation in the direct path. This 3 dB can be removed, under software control, to provide some up-fade capability. The unfaded outputs at the alternative frequency of 1.070 GHz are designed for a level of −15 dBm.

Finally, test ports are provided to permit frequency response measurements of each variable network prior to the 1.070-GHz bandpass filter. The signal level at each of these ports is nominally −52 dBm.

6.3 Software accuracy: matching the model statistics

Using the methods described in Section 5.1, random variations for each parameter of the Rummler space diversity model were generated. Figures 17 and 18 show the distributions of the uniform variation, and the Rayleigh plus exponential variation representing B_{horn}. B_{horn} was nonlinearly transformed to produce, in theory, a linear distribution function. This check on the accuracy was performed and the result, not shown, was very nearly linear.

The distributions were obtained from a single variation containing 50,000 samples, which corresponds to about 1666 independent samples for the ACF used. Similar results were obtained for the other fade parameters but are not shown for brevity.

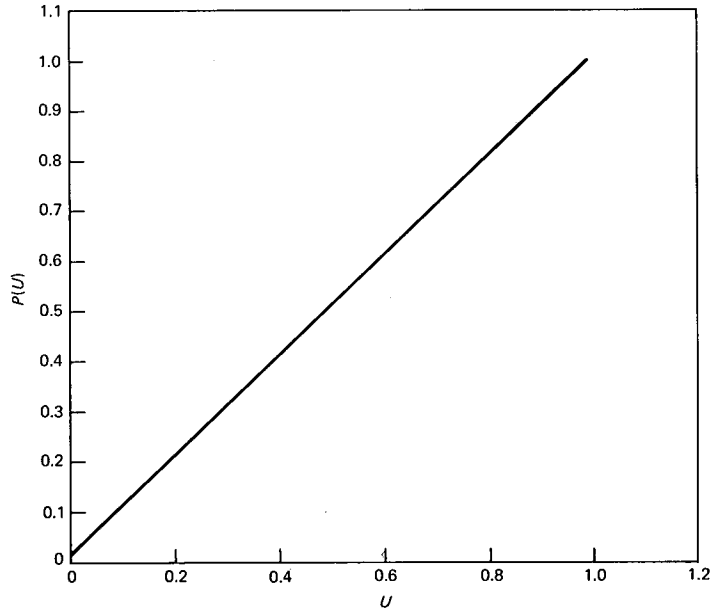

Fig. 17—Distribution of the underlining uniform for B_{horn}.

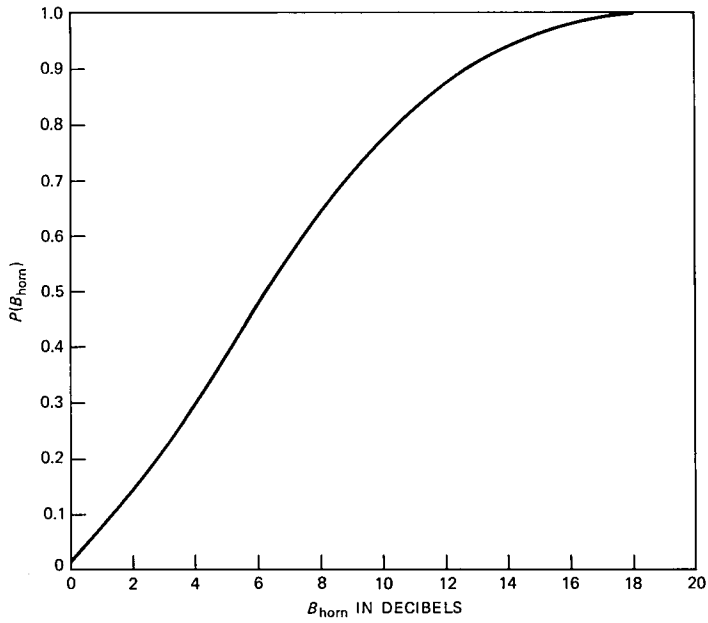

Fig. 18—Final distribution of the B_{horn} parameter.

For the pedestal-type density functions for ϕ, accuracy was checked directly by measuring the slopes of the final distribution functions. This yielded the desired values of 5 and 8 for the density function pedestal ratios for the Horn and Dish Channels. The A parameter distributions were checked using the same Gaussian-to-uniform transformation as in the generation procedures for B and ϕ. Again, a linear plot should result and was obtained.

The ACFs for B_{dish} are shown in Fig. 19. The time separation among ACFs for the underlying Gaussian, uniform, and final variations is about 2 seconds for this parameter. Results for B_{horn} and the ϕ parameters are similar but show less variation. The underlying Gaussians variations were adjusted so that their ACFs agree with the fade model ACFs at the 1/e points.

The ACF for the Gaussian variations of A_{horn} and A_{dish} must be the same so that the resulting distributions both follow the required ACF. Therefore, the ACF time constants for the Horn and Dish Channels are set equal and adjusted together. It was found that changes in ACF resulted when the A parameters were correlated and then each was biased by a mean related to B, as specified by the model. This is shown in Fig. 20.

Figures 21 through 23 show the differences between a smoothed version of the prescribed Rummler single-channel ACFs and the

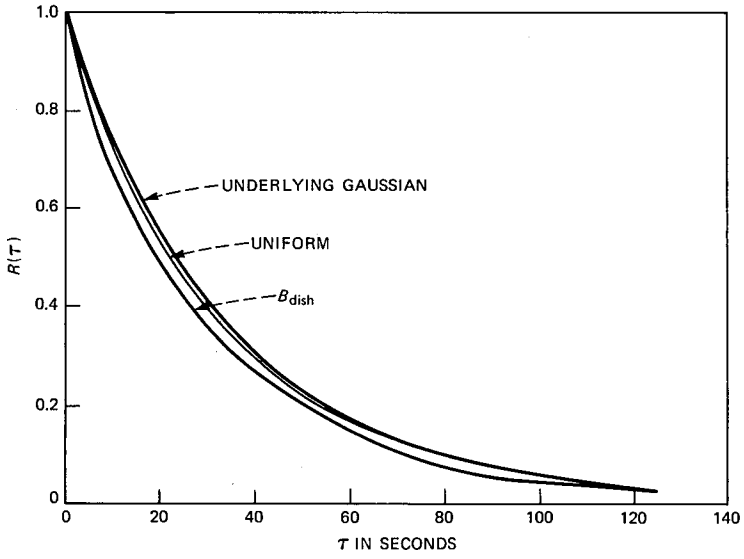

Fig. 19—ACF for the underlying Gaussian, uniform and B_{dish}.

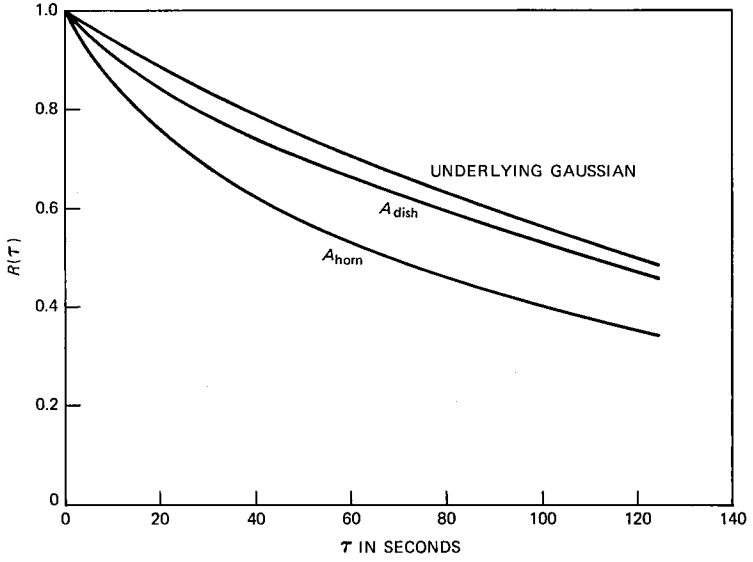

Fig. 20—ACF for the underlying Gaussian, A_{dish} and A_{horn}.

resulting ACFs for the Horn and Dish Channels for each of the A, B and ϕ parameters, respectively. The agreements are quite good.

Thus, we have carried out our parameter generation method for the Rummler dual channel space diversity model and have verified its

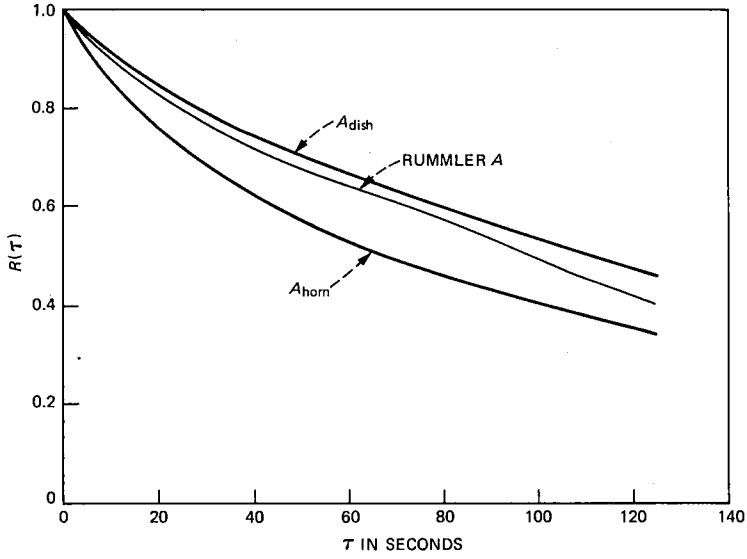

Fig. 21—Comparison of desired Rummler ACF with measured ACF for A_{horn} and A_{dish}.

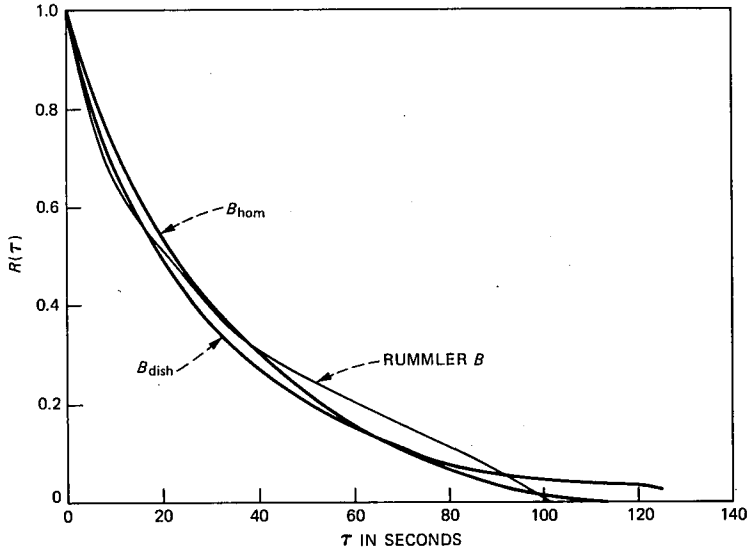

Fig. 22—Comparison of desired Rummler ACF with measured ACF for B_{horn} and B_{dish}.

accuracy. For reasonable PDFs, our iterative procedure yields a random variation whose ACF is close to the desired ACF when the latter is applied to the underlining Gaussian variation. The B and ϕ parameters showed little variation or no variation after the nonlinear func-

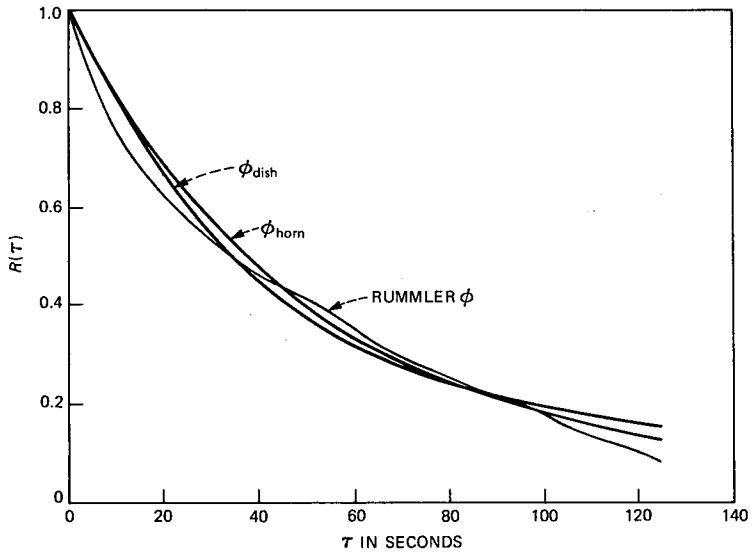

Fig. 23—Comparison of desired Rummler ACF with measured ACF for ϕ_{horn} and ϕ_{dish}.

tions were applied. The A parameter (which does not use the iterative generation method) showed a modest variation due to the addition of the mean which is related to the B parameter. Finally, the PDFs of the generated parameters have been shown to agree with the PDFs specified by the model.

6.4 Hardware accuracy: matching the intended responses

In this subsection, we assess the accuracy with which the simulation hardware produces the responses called for by the software. We begin by discussing appropriate error measures and end with experimental results.

6.4.1 General approach

Consider any one of the variable channel networks, i.e., the Horn Channel or Dish Channel of a given DCU. The input control variables (A, C, and θ) to this network at any instant are intended to produce a short-term frequency response [see (2), (4), and (5)] given by

$$H(f) = 10^{A/20} + 10^{C/20}e^{j\theta}e^{-j\omega\tau}. \tag{10}$$

As the control variables change slowly, $H(f)$ is meant to change slowly, too, in accordance with this equation.

Now suppose that, for given A, C, and θ, we measure the *actual* response of the network, $H_0(f)$, and compute some index of its depar-

ture from the *intended* response, (10), over some bandwidth. For example, we could compute

$$\epsilon = \overline{|H(f) - H_0(f)|^2} / \overline{|H(f)|^2}, \tag{11}$$

where the overbar denotes a frequency integration from, say, −20 MHz to +20 MHz. Next, suppose that ϵ were computed at fixed intervals in time as A, C, and θ moved slowly through their computer-generated variations. We could then obtain a population of ϵ-values and compute a cumulative distribution, $P(\epsilon)$. If the joint variations of A, C and θ for this experiment were representative of a particular statistical fading model, we could say that $P(\epsilon)$ is the error-measure distribution, over the *fade response ensemble* of that model, of the variable network. Finally, a set of such distributions for all four variable networks could be used to characterize—for that particular model—the accuracy of the simulator hardware.

6.4.2 Specific error measures

We devised an experimental procedure similar to the one just described, and used it to evaluate each of the variable channel networks of the CSF. In so doing, we used the dual diversity channel model of Rummler[7] to derive the fade parameter variations. At the same time, we made two important changes in the error measure, which we now discuss.

First, we chose, for the sake of simplicity, to avoid measuring the complex response $H_0(f)$; instead, we measured its squared magnitude (amplitude response) only. This function can be usefully compared with the squared magnitude of $H(f)$, (10), by means of the following error measure:

$$\epsilon(A, C, \theta) = \overline{[(G(f) - G_0(f))/G(f)]^2} \,|\, \{A, C, \theta\}, \tag{12}*$$

where

$$G(f) \triangleq |H(f)|^2; \qquad G_0(f) \triangleq |H_0(f)|^2, \tag{13}$$

and the frequency averaging is over the specified bandwidth. Given the uncomplicated nature of the frequency-selective networks, we assert that little is lost by omitting phase response data from the error measures; amplitude response accuracy alone is a reliable indicator of how well $H_0(f)$ matches $H(f)$.

It can be shown that the above error measure can be used to approximate quite closely the *root mean square decibel error* between

* We show the control variables A, C and θ here to make their pertinence explicit. Henceforth, we shall suppress them.

$G(f)$ and $G_0(f)$, as averaged over the specified bandwidth. Specifically, this quantity is approximated by $(4.34\sqrt{\epsilon})$ dB for all $\epsilon \leq 0.2$.

Our second change was to separate the error measure into a *scale error* and a *shape error*.* This approach acknowledges the fact that a small *scale* difference between $G(f)$ and $G_0(f)$ (i.e., a small *level* difference in their decibel variations) would be relatively unimportant given the vagaries of transmitter power, free space path loss, receiver noise figure, and other link power quantities. We estimate that pure level differences lying within ±1 dB would be quite acceptable in view of these factors.

Accordingly, we modify ϵ in (12) so as to permit a scaling of $G_0(f)$ by an "optimal" factor, r_{opt}, to be defined shortly. The value of ϵ with this scaling incorporated is then a measure solely of the *shape* difference between the intended and measured responses. The mathematics follows.

We define ϵ to be

$$\epsilon = \min_r \{\overline{[(G(f) - rG_0(f))/G(f)]^2}\}. \tag{14}$$

The minimizing r, which we define to be optimal and call r_{opt}, is easily found to be

$$r_{opt} = \frac{\overline{(G_0(f)/G(f))}}{\overline{(G_0(f)/G(f))^2}} \tag{15}$$

and the resulting ϵ is

$$\epsilon = 1 - \frac{\overline{[(G_0(f)/G(f))]^2}}{\overline{(G_0(f)/G(f))^2}}. \tag{16}$$

For a given A, C and θ, the quantity

$$R = 10 \log_{10}(r_{opt}) \tag{17}$$

is the *scale error* of the variables network, in decibels, for these control variables; and the quantity

$$\sigma \cong (10/\ell n\ 10)\sqrt{\epsilon} \tag{18}$$

estimates the root-mean square decibel shape error (or just *shape error*) of the variable network for these control variables. A conservative accuracy requirement is that these quantities lie within ±1 dB and below 0.5 dB, respectively, over all likely combinations of the control variables.

---

* If the power responses $G(f)$ and $G_0(f)$ are replaced by their decibel equivalents, this separation is akin to isolating the "dc" and "ac" error variations with respect to f.

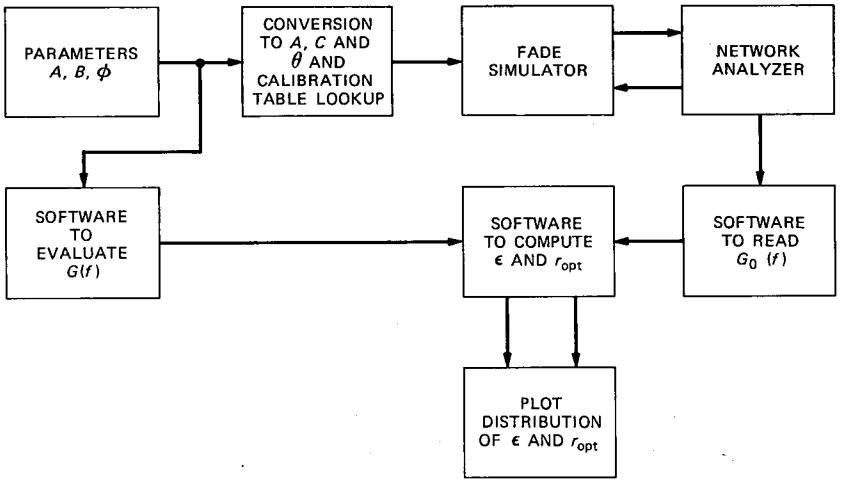

Fig. 24—Block diagram of error measurement.

6.4.3 Results

The error measures defined above were obtained for each of the four variable channel networks of the CSF. The results can be regarded as more than a check on the hardware alone. They also reflect on the accuracy of the software translations into electrical signals, the lookup routines and tables, and the software that generates those tables.

The hardware and software test configuration is shown in Fig. 24. The control computer first calculates the magnitude of the desired responses $G(f)$, from the down loaded files containing A, B, and ϕ parameters. These files are also used to generate the binary A, C, and θ values for the D/A converters by transformations and lookup tables as previously discussed. The D/A converters are loaded with the binary values and after a delay to allow the lowpass filters on the D/A control lines to settle, the response of the channel, $G_0(f)$, is sampled at 40 frequencies spaced at 1-MHz intervals over the specified bandwidth. These frequency samples are compared to the calculated samples, and error measures are computed and saved on a disk. Specifically, for each time sample of $G(f)$ and $G_0(f)$, we computed ϵ and r_{opt} using (16) and (15). In doing so, we used numerical-sum approximations to the continuous-frequency integrations called for in these equations. Given the smooth frequency responses produced by the variable channel networks, we found the 1-MHz spacings between measured values of G and G_0 to be quite adequate.

The final step in the procedure was to obtain, for each network, a cumulative distribution from the 7200 values of ϵ, and another for r_{opt}. Results for r_{opt} are given in Fig. 25 for the Horn and Dish Channels

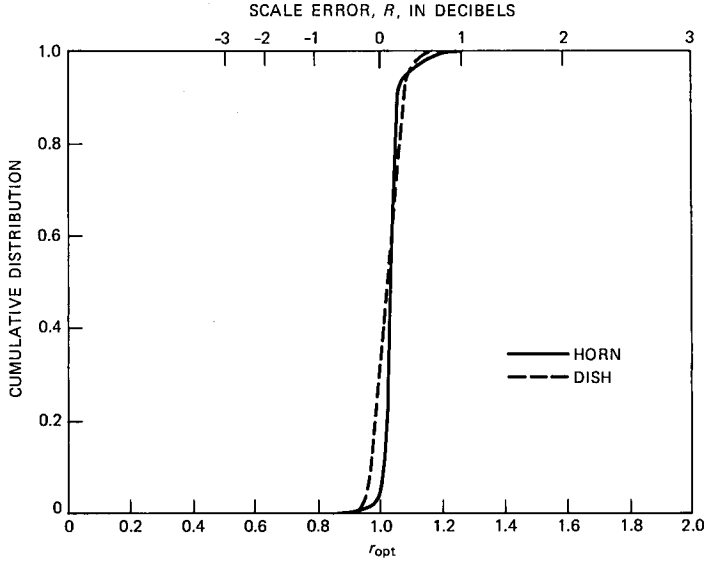

Fig. 25—Cumulative distributions of scale error, R, for each channel of a dual channel unit.

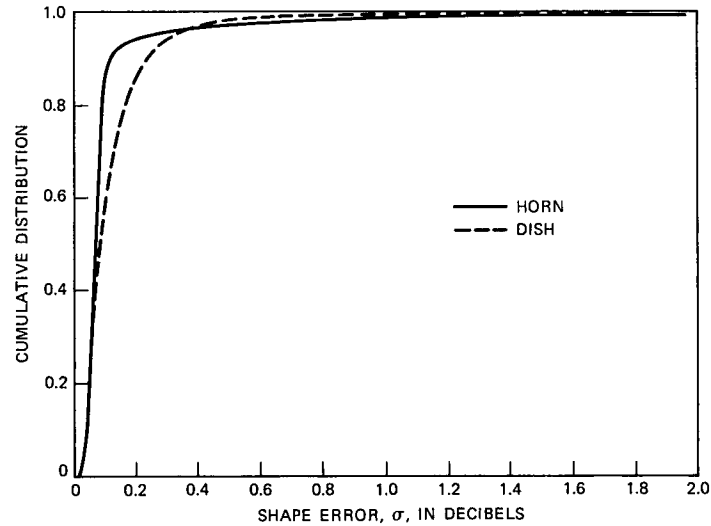

Fig. 26—Cumulative distributions of shape error, σ, for each channel of a dual channel unit.

of one of the DCUs; the corresponding results for ϵ [converted to σ via (18)] are given in Fig. 26. Very similar results were obtained for the other DCU. There are small but discernible differences between the distributions for the Horn and Dish Channels. Mostly, these are due

to the slightly different multipath fading histories generated for these two channels by the software.

The important findings from Figs. 25 and 26 are that the scale error (R) lies well within ±1 dB over all fades and that the root-mean-square decibel error (or shape error, σ) lies below 0.5 dB for over 98 percent of all fades. This is true for all four networks of the CSF and is the result we wanted. The accuracy of the hardware is thus confirmed.

VII. CONCLUSION

We have described a CSF capable of providing the radio system designer with means of measuring and comparing performance of new or existing radio hardware over multipath channels without field installation on a real path. The ability to replay a fade ensemble repeatedly in a test instead of waiting for the perversity of nature makes this simulation technique very attractive.

VIII. ACKNOWLEDGMENT

The authors want to thank M. F. Wazowicz for his help in hardware assembly and E. C. Cox, P. Knoetgen and V. R. Dillard for their help in the development of control software. We also want to especially thank L. J. Greenstein and Y. S. Yeh for their generous advice and support in both design and documentation of the simulation facility.

REFERENCES

1. W. T. Barnett, "Multipath Propagation at 4, 6 and 11 GHz," B.S.T.J., *51,* No. 2 (February 1972), pp. 321–61.
2. W. D. Rummler, "A New Selective Fading Model: Application to Propagation Data," B.S.T.J., *58,* No. 5 (May–June 1979), pp. 1037–71.
3. L. J. Greenstein and B. A. Czekaj, "A Polynomial Model for Multipath Fading Channel Responses," B.S.T.J., *59,* No. 9 (September 1980), pp. 1197–225.
4. W. D. Rummler, "More on the Multipath Fading Channel Model," IEEE Trans. Commun., *COM-29,* No. 3 (March 1981), pp. 346–52.
5. M. Liniger, "Sweep Measurements of the Transferfunction of an RF-Channel and Their Representation by Polynomials," Intl. Conf. Commun., Philadelphia, Penn., June 13–17, 1982, paper 7B3.
6. L. Martin, "Statistical Results on Selective Fading," Intl. Conf. Commun., Philadelphia, Penn., June 13–7, 1982, paper 7B5.
7. W. D. Rummler, "A Statistical Model of Multipath Fading on a Space Diversity Radio Channel," B.S.T.J., *61,* No. 9, Part 1 (November 1982), pp. 2185–219.
8. W. D. Rummler, "A Rationalized Model for Space and Frequency Diversity Line-of-Sight Radio Channels," Int. Conf. Commun., June 19–22, 1983, Boston, Mass., paper E27.
9. K. T. Wu, "Measured Statistics on Multipath Dispersion of Cross Polarization Interference," Intl. Conf. Commun., May 14–7, 1984, Amsterdam, paper 46.3.
10. M. H. Meyers, "Multipath Fading Characteristics of Broadband Radio Channels," GLOBECOM '84, Atlanta, Ga., November 26–29, 1984, paper 45.1.
11. M. Liniger, "Sweep Measurements of Multipath Effects on Cross-Polarized RF-Channels Including Space Diversity," GLOBECOM '84, Atlanta, Ga., November 26–9, 2984, paper 45.
12. L. J. Greenstein and V. K. Prabhu, "Analysis of Multipath Outage With Applications

to 90 Mbit/s PSK Systems at 6 and 11 GHz," IEEE Trans. Commun., *COM-27*, No. 1 (January 1979), pp. 68–75.
13. W. C. Jakes, Jr., "An Approximate Method to Estimate an Upper Bound on the Effect of Multipath Delay Distortion on Digital Transmission," IEEE Trans. Commun., *COM-27*, No. 1 (January 1979), pp. 76–81.
14. R. P. Coutts and J. C. Campbell, "Mean Square Error Analysis of QAM Digital Radio Systems Subject to Frequency Selective Fading," A.T.R., *16*, No. 1, 1982, pp. 23–38.
15. L. J. Greenstein and B. A. Czekaj-Augun, "Performance Comparisons Among Digital Radio Techniques Subjected to Multipath Fading," IEEE Trans. Commun., *COM-30*, No. 5 (May 1982), pp. 1184–97.
16. G. J. Foschini and J. Salz, "Digital Communications Over Fading Radio Channels," B.S.T.J., *62*, No. 2, Part 1 (February 1983), pp. 429–56.
17. D. P. Taylor and M. Shafi, "Fade Margin and Outage Computation of 4ϕ-QPRS Radio Employing Decision Feedback Equalization," Intl. Conf. Commun., Boston, Mass., June 19–22, 1983, paper F2.1.
18. O. Andrisano, "The Combined Effects of Noise and Multipath Propagation in Multilevel PSK Radio Links," IEEE Trans. Commun., *COM-32*, No. 4 (April 1984), pp. 411–8.
19. N. Amitay and L. J. Greenstein, "Multipath Outage Performance of Digital Radio Receivers Using Finite-Tap Adaptive Equalizers," IEEE Trans. Commun., *COM-32*, No. 5 (May 1984), pp. 597.
20. W. C. Wong and L. J. Greenstein, "Multipath Fading Models and Adaptive Equalizers in Microwave Digital Radio," IEEE Trans. Commun., *COM-32*, No. 8 (August 1984), pp. 928–34.
21. N. Amitay and J. Salz, "Linear Equalization Theory in Digital Data Transmission Over Dually Polarized Fading Radio Channels," AT&T Bell Lab. Tech. J., *63*, No. 10, Part 1 (December 1984), pp. 2215–59.
22. L. J. Greenstein and Y. S. Yeh, "A Simulation Study of Space Diversity and Adaptive Equalization in Microwave Digital Radio," AT&T Tech. J., *64*, No. 4 (April 1985), pp. 885–905.
23. M. Emshwiller, "Characterization of the Performance of PSK Digital Radio Transmission in the Presence of Multipath Fading," ICC78, June 1978, Paper 47.3.
24. C. W. Lundgren and W. D. Rummler, "Digital Radio Outage Due to Selective Fading-Observation vs. Prediction from Laboratory Simulation" B.S.T.J., *58*, No. 5 (May–June 1979), pp. 1073–1100.
25. Y. Y. Wang, "Simulation and Measured Performance of a Space Diversity Combiner for 6 GHz Digital Radio," IEEE Trans. Commun., *COM-27*, No. 12 (December 1979), pp. 1896–1907.
26. S. T. Matsuura, "Estimated Performance of a QPR Digital Microwave Radio in the Presence of Frequency Selective Fading," Intl. Conf. Commun., Philadelphia, Penn., June 13–7, 1982, paper 7B2.
27. J. C. Campbell and R. P. Coutts, "Outage Prediction of Digital Radio Systems," Electron. Lett., *18*, No. 25/26, December 1982, pp. 1071–2.
28. A. L. Martin, R. P. Coutts and J. C. Campbell, "Results of a 16 QAM 140 Mbit/s Digital Radio Field Experiment," Intl. Conf. Commun., Boston, Mass., June 19–22, 1983, paper F2.2.
29. C. P. Bates and M. A Skinner, "Impact of Technology on High Capacity Digital Radio Systems," Intl. Conf. Commun., Boston, MA, June 19–22, 1983, paper F2.3.
30. S. Barber, "Cofrequency Cross-Polarized Operation of a 91 Mb/s Digital Radio," IEEE Trans. Commun., Vol. COM-32, No. 1, January 1984, pp. 87–91.
31. M. H. Meyers, "Multipath Fading Outage Estimates Incorporating Path and Equipment Characteristics," GLOBECOM '84, Atlanta, Ga., November 26–9, 1984, paper 45.2.
32. M. M. Sondhi, "Random Processes With Specified Spectral Density and First Order Probability Density," B.S.T.J., *62*, No. 3 (March 1983), pp. 679–702.
33. G. Vannucci and M. C. Teich, "Computer Simulation of Superposed Coherent and Cohaotic Radiation," Applied Optics, *19*, No. 4 (February 15, 1980), pp. 548–53.
34. W. D. Rummler, "Advances in Multipath Channel Modeling," Intl. Conf. Commun., Seattle, Wash., June 8–12, 1980, 52.3.1.

AUTHORS

Harold H. Hoffman, New York University; AT&T Bell Laboratories. Mr. Hoffman, a member of the Radio Systems Research Department, has worked

on microwave radio relay systems, cordless telephone, satellite orientation, mobile radio, millimeter wave propagation, and a 7-meter radio astronomy receiver and antenna. He holds patents for IF amplifier design and signal processing. He is presently concerned with digital radio fading simulators and mobile radio propagation studies.

R. S. Roman, AT&T Bell Laboratories, 1970—. Mr. Roman, a member of the Radio Systems Research Department, has been concerned with digital radio system studies. He is currently a student at Brookdale Community College.

A. J. Rustako, Jr., B.S.E.E. 1965, M.S.E.E. 1969, New Jersey Institute of Technology; AT&T Bell Laboratories, 1957—. Mr. Rustako, a member of the Radio Systems Research Department, has been engaged in radio system and propagation studies. He contributed to early work in UHF and microwave mobile radio communications, in particular, propagation measurements of the multipath medium, and the use of diversity techniques. He has also made contributions in the field of satellite communications. These include earth-space propagation measurements of rain attenuation and depolarization at 12 GHz, and the use of phased array techniques for rapid scanning spot beam satellite antennas. He is presently concerned with high-speed digital radio transmission techniques.

Clark B. Woodworth, B.S.E.E., 1977, Monmouth College; M.S.E.E., 1980, Rutgers University; AT&T Bell Laboratories, 1977—. Mr. Woodworth worked in the Satellite Systems Research Department and the Radio Systems Research Department. Work in the latter department included digital radio studies and multipath channel simulation. He is currently working in the Network Systems Research Department. Member, Eta Kappa Nu, Sigma Pi Sigma, IEEE.